Advances in Science and Technology
ISSN: 1662-0356, Vol. 145, pp 131-139
doi:10.4028/p-EV4gPv

Submitted: 2023-07-03
Revised: 2023-11-17
Accepted: 2023-11-24
Online: 2024-03-29

Calculating Rheological Properties of Fresh Mortar for Additive Manufacturing Based on Experimental, Multi-Sensor Data

E. Schönsee[1,a*], G. Hüsken[,1,b], A. Jeyifous[1,c] A. Mezhov[1,d], C. Strangfeld[1,e]

Bundesanstalt für Materialforschung und -prüfung (BAM), Unter den Eichen 87, 12205 Berlin, Germany

[a]eric.schoensee@bam.de, [b]goetz.huesken@bam.de, [c]anthony.jeyifous@bam.de, [d]alexander.mezhov@bam.de, [e]christoph.strangfeld@bam.de

Keywords: 3DCP, Concrete Printing, Additive Manufacturing, Monitoring, Rheology, Bingham Fluid

Abstract. Additive manufacturing of concrete structures is a novel and emerging technology. Free contouring in civil engineering, which allows for entirely new designs, is a significant advantage. In the future, lower construction costs are expected with increased construction speeds and decreasing required materials and workers. However, architects and civil engineers rely on a certain quality of execution to fulfil construction standards. Although several techniques and approaches demonstrate the advantages, quality control during printing is highly challenging and rarely applied. Due to the continuous mixing process commonly used in 3D concrete printing, it is impossible to exclude variations in the dry mixture or water content, and a test sample cannot be taken as a representative sample for the whole structure. Although mortar properties vary only locally, a defect in one layer during printing could affect the entire integrity of the whole structure . Therefore, real-time process monitoring is required to record and document the printing process.
At the Bundesanstalt für Materialforschung und -prüfung (BAM) a new test rig for the additive manufacturing of concrete is built. The primary purpose is measuring and monitoring the properties of a mortar during the printing process.
The following study investigates an approach for calculating yield stress and plastic viscosity based on experimentally recorded pressure data. The calculations assume that fresh mortar behaves as a Bingham fluid and that the Buckingham-Reiner-equation is applicable. A test setup consisting of rigid pipes with integrated pressure sensors at different positions is utilized.
Monitoring the printing process with different sensors is crucial for the quality control of an ongoing process.

Introduction

For 3D concrete printing (3DCP), it is a common approach to continuously mix fresh mortar and bring it into a hose. The hose leads to a nozzle which is connected to a mechanical system so the material can be placed in different layers for building up a structure. Different case studies show multiple accomplishments in this field. Most of them were focusing on building representative elements [1, 2]. Salet et al. have presented a case study where an infrastructural element, a bridge for pedestrians, was built [3]. Also in fields of building houses, 3DCP is of high interest because of the possibility to save human resources and time [4]. Today, 3DCP is a tiny niche market and large-scale application remains questionable because no standards exist so far. To change that, standards need to be developed and a quality control of the constant mixing process is required, because a single sample of material cannot be taken as representative, if mixing happens continuously.
As an approach to a continuous monitoring system of the fresh mortar, multiple sensors were integrated into a rigid pipe, which can be placed at the side of the printer itself [5]. In a first step, pressure and temperature are observed in multiple positions. Assuming that the mortar for 3DCP behaves as a Bingham fluid, it can be assumed further, that plug flow occurs in the tube and that the Buckingham-Reiner equation (as shown in Eq. (1)) could be applicable [6, 7]. The Buckingham-Reiner equation says that the volume flow Q in $\mathrm{m^3 s^{-1}}$ can be calculated if the pressure loss ΔP in $\mathrm{kgms^{-2}}$ for a tube

with a known geometry in terms of length l in m and inner radius r_{pipe} in m, the plastic viscosity μ in kgm^{-1}s^{-1} and the minimum pressure p in kgms^{-2} which is needed for flow are known.

$$Q = \frac{\pi r_{pipe}^4}{8\mu l}\left(\Delta P - \frac{4}{3}p + \frac{p^4}{3\Delta P^3}\right) \tag{1}$$

Furthermore, Sakuta et al. have proposed to calculate the rheological properties from different states of volume flow rate [8]. With the aim of doing that, $\kappa = \frac{P_1 Q_2}{P_2 Q_1}$ and $\varepsilon = \frac{P_2}{P_1}$ have been introduced. With $\alpha = \frac{p}{\Delta P} = \frac{r_{plug}}{r_{pipe}}$ and the assumption of two states of volume flow, they showed that Eq. (1) could be written as shown in Eq. (2).

$$1 - \frac{4\alpha}{3\varepsilon} + \left(\frac{{\alpha_1}^4}{3\varepsilon}\right) = \kappa\left(1 - \frac{4\alpha_1}{3} + \frac{\alpha_1^4}{3}\right) \tag{2}$$

Tattersall et al. also have shown the relation of yield stress τ in kgm^{-1}s^{-2}, pressure loss in kgms^{-2}, length of the pipe l in m and radius of the pipe r_{pipe} in m as seen in Eq. 3 [6]. Hence, if α can be calculated from Eq. (2), further calculations on rheological parameters are possible.

$$\frac{\Delta P}{l} = \frac{2\tau_0}{r_{pipe}\alpha} \tag{3}$$

In the following, an experimental setup is introduced to investigate, if the Buckingham-Reiner equation could be a suitable approach for quality control in 3DCP.

Design of Experiments

With the scope of investigations on a non-reactive mortar, a setup was built that allows pumping in a circuit. The pump is a 'm-tec duomix connect' which consists of a reservoir for dry material, a mixing unit where water is added and the mortar is mixed, a reservoir for fresh mortar and a worm pump which pumps the material into a hose. To ensure that the material is mixed homogeneously and variations in water content can be minimised, the internal mixing unit was not in use. The material was prepared in a batch mixer and was filled manually into the reservoir of the pump. Going downstream, the pipe consists of flexible and rigid elements, which were connected by mortar couplings. Around 0.7 m downstream of the pump, a temperature sensor (PT100) was integrated. After a short, flexible hose, a rigid steel pipe with 4 pressure sensors followed. To avoid mechanical damage, the pressure sensors are protected by a diaphragm seal. The steel pipe consists of two straight pipes, one with the length of 2.5 m and the second with a length of 1 m, connected with a pipe bend of 90°. After a second pipe bend, another flexible hose and another PT100 were placed. The distance between the sensors composes of the pipe length, the couplings and the sensor modules and can be seen in Fig. 1. The flexible hose is connected to the top of the pump reservoir to lead the material back and to close the circuit. The inner diameter of the hole supply system, rigid pipes and flexible tubes, is 25 mm, with slight variations were mortar couplings are in use. The radius of the pipe bend is 200 mm.
To avoid hydration during the experiments, different non-reactive mixes based on uncompacted limestone powder were used. Natural river sand was used as fine aggregate in different size fractions. To achieve variations in rheological properties, water content was changed for each mixture. The composition can be seen in table 1. Penetration tests have shown no variations in 24 hours, so the material can be classified as non reactive and suitable for the experiments of this study [5].
To characterise material properties, additional experiments has been performed. Air content has been determined according to DIN EN 1015-7 [9]. Before air content measurements were performed, the sample container was used to weigh the material with a known volume and determine the density of the mortar. For determination of the rheological properties of the limestone mortars, a sample of material was taken before the pumping experiments. The sample was analysed with a 'Schleibinger Viscomat NT' with basket cell setup. The experiments were performed as suggested in [10]. To allow

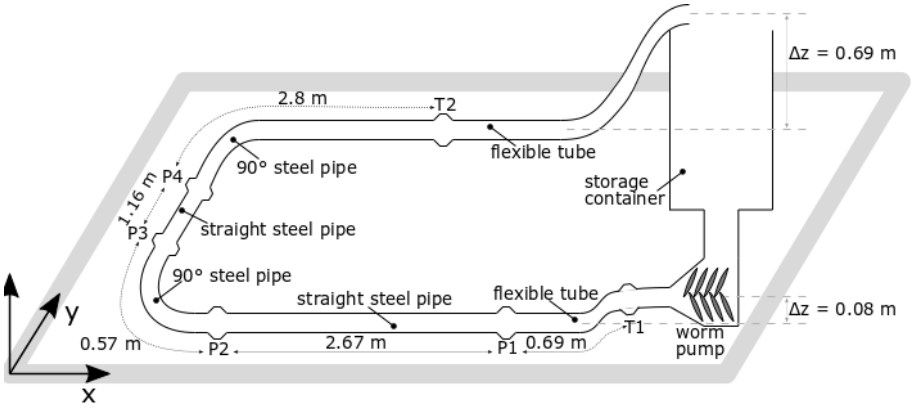

Fig. 1: Sketch of the experimental setup [5]

for a comparison with conventional test methods, the spread flow was determined according to DIN EN 1015-3 [11].

Table 1: Composition of non-reactive limestone mixtures for pumping tests

Mixture	Mix A	Mix B	Mix C	Mix D	Mix E
Limestone powder in $[kg]$ per $[m^3]$	650				
Micro silica in $[kg]$ per $[m^3]$ Elkem Microsilica®940U	45.5				
Sand (0.1 ... 0.5) mm in $[kg]$ per $[m^3]$	780.2				
Sand (0.5 ... 1.0) mm in $[kg]$ per $[m^3]$	350.1				
Water in $[kg]$ per $[m^3]$	308.8	313	325	273	330
Superplasticiser in $[kg]$ per $[m^3]$ MasterGlenium Sky 591	3.77		2.48	3.77	
Starch-based stabiliser in $[kg]$ per $[m^3]$ Foxcrete S 100-F	0.65				

To acquire data on volume flow, the mass flow was calculated manually by weighing the output of material during a period of time for different levels of pump speed during the experiment. The time was taken by a stopwatch. The volume flow itself was calculated afterwards from the determined density of the material.

Pressure and temperature data was acquired and monitored continuously and automatically. The data acquisition system consists of the sensors, a repeater power supply which transmitted the signal from 4...20 mA to 2...10 V, (respectively a temperature transmitter for the PT100, which was configured to transmit 0...50 °C to 0...10 V) and a NI USB 6210. The data acquisition device (DAQ) was connected to a computer which runs a LabVIEW program. The Data is saved with a sampling rate of 10 Hz

In the beginning of the pumping procedure, a low viscous limestone suspension was filled into the pump to avoid mechanical damage of the worm pump. After the reservoir was empty, the limestone mortar was inserted. To minimize the effect of the suspension, the circuit of the tube system was kept open in the beginning and the suspension was obtained until just limestone mortar was taken from the outlet. Afterwards, the system outlet is placed into the storage container of the pump to enable pumping in a circuit. During the experiments, different levels of pump speed were applied. The mass

flow was measured for 20 %, 50 % and 80 % of pump speed. In Fig. 2 the data for one experiment is visualised as an example. The area which is marked up green is where the system got filled up with limestone suspension and mortar. Afterwards, a pumping procedure with varying pumping speed was performed. Higher pump speed leads to higher volume flow, which corresponds to a higher pressure inside of the system. The pump speed was increased gradually up to 80 %. Afterwards, the pump speed was decreased and increased in an alternating way. For that experiment, the same pattern was repeated three times. The variation of pump speed can be seen clearly in the signals of the pressure sensors. At the end of data acquisition, the blue markup indicates the flow measurements. The acquisition of volume flow always happened at the end of the experiments. Also, a fast increase in temperature sensor T1 can be noticed, that occurs always shortly after switching on the worm pump. Also, after a short period of time, the temperature at the second temperature sensor T2 increases slightly. During pumping, heat is generated due to friction in the worm pump, and which heats up the pumping section. Consequently, the heat transfer to the mortar is higher when the pump is stopped, and the temperature of the mortar is increasing. The short temperature increase is recorded by the sensors as soon as the pumping continues.

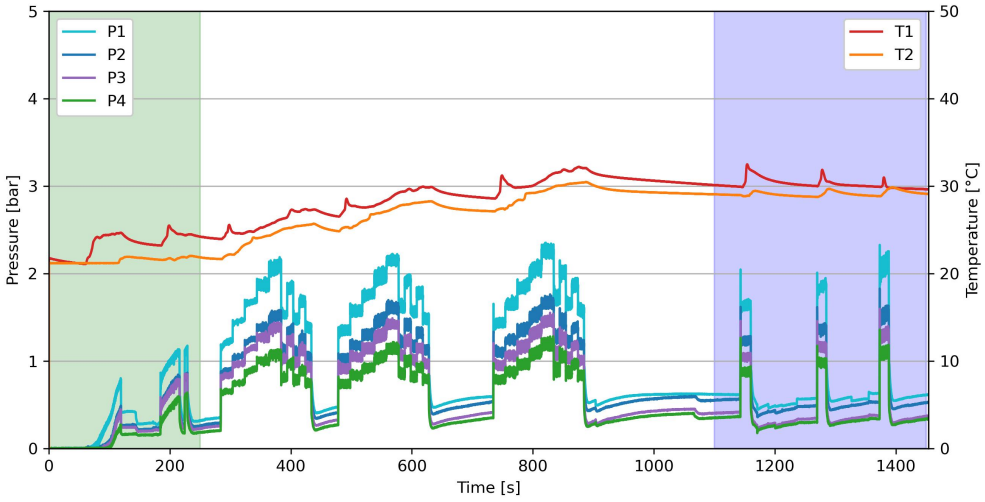

Fig. 2: Example for pressure and temperature data on a pumptest

Discussion of Experimental Results

Uncertainty of measurement. To allow a quantification of the uncertainty of measurement it is referred to the Guide to the Expression of Uncertainty in Measurement (GUM) [12]. The calculations of the uncertainty of the system are performed according to type B evaluation of standard uncertainty. First, the temperature sensors are to be considered. The uncertainty of the PT100 with a class of tolerance A can be found in DIN EN 60751 [13]. Expanded uncertainties of other devices are taken from corresponding data sheets. The extended uncertainty of the pressure sensors calculates to $U_P = 0.2\,bar$ and the uncertainty of the temperature sensors to $U_T = 0.6\,K$. A summary of the uncertainties of the different devices is given in Table 2. According to GUM, the combined standard uncertainty is calculated as shown in Eq. 4 [12]. For the pressure drop from one sensor to another, this leads to a standard uncertainty of $u_{\Delta P} = 0.14\,bar$. The standard uncertainty of the distance between two pressure sensors is assumed to be $u_l = 0.01\,m$. If length of the pipe is taken into account and the pressure drop per meter is calculated, the uncertainty of the measurements for pipe section A calculates to $u_{\Delta P/l_A} = 0.05\,bar/m$.

Considering a coverage factor of $k = 2$, the expanded uncertainty is given with $U_{\Delta P/l} = 0.1\,bar/m$. Respectively for section B of the system, the expanded uncertainty calculates to $U_{\Delta P/l_B} = 0.24\,bar/m$.

$$u_c^2(y) = \sum_{i=1}^{N} \left(\frac{\delta f}{\delta x_i} \right) u^2(x_i) \tag{4}$$

Table 2: List of expanded uncertainties, standard uncertanties and coverage factor

Device	Expanded Uncertainty U	Coverage factor k	Standard Uncertainty u
DAQ	229 μV	3	76.33 μV
Temperature transmitter	0.125 K	2	0.0625 K
PT100	0.19 K	2	0.095 K
Power Repeater Supply	0.01 bar	2	0.005 bar
Pressure Sensors	0.2 bar	2	0.1 bar

Summary of testing. The different results for density, flow table testing and the results from viscomat-tests are listed in table 3 and will be compared to the calculations done on pressure loss and volume flow measurements.

Table 3: Summary of external testing

Mixture	Mix A	Mix B	Mix C	Mix D	Mix E
Density [kg m^{-3}]	2072	2072	2107	2085	2107
Air content [%]	2.9 %	3.1 %	2.8 %	1.1 %	4.0 %
Flow table testing [mm]	115/214.25	122/225.5	116.25/217.25	105/197	148.8/248.75
Yield stress [Pa]	195.6	119	149.6	239.1	14.43
Plast. Viscosity [Pa s]	3.76	4.07	4.51	3.19	5.43

Pressure loss is determined for the same time when the flow measurements were performed. The pressure loss between the for pressure sensors is normalised by the length of the individual pipes to allow for a better comparison. To exclude influence due to starting and stopping the pump, the mean value of the plateau that evolved was taken for calculations, but the first and the last second were not considered. In table 4 the variations of pressure loss at the two steel pipes and the taken volume flow measurements are listed. The distance between P1 and P2 is referred to as section A, respectively the distance between P3 and P4 as section B. The percentage of pump speed can be identified by the index as well. As it would be expected, the data shows that pressure loss is rising corresponding to a rising volume flow. It is seen, that the pressure losses vary for pipe A and pipe B, even though they are normalized for the length of the pipe. It is assumed that the bend of the pipe is influencing the flow profile in the pipe, which would have an impact on the pressure level in P3, right behind the bend.

Comparing of yield stress. With given values for pressure loss between two sensors measured in a straight and rigid pipe, κ and ε can be calculated according to [6]. If those are known, the calculation of α can be done by solving Eq. (2). It is an obvious constraint that, if plug flow occurs, $\alpha = r_{plug}/r_{pipe}$ has to be larger than 0 and lower than 1, because of the geometry of the pipe. If α is calculated, the calculation of τ_0 and μ can be performed.

These calculations are performed numerically by a simple python code. The results for the calculation of yield stress can be seen in Fig. 3. The viscomat data, seen in 3, is applied to the x-axis, the y-axis shows the calculated yield stress. In Fig. 3 the data is plotted in different sub-figures for different variations of pump speed and pipe sections. It is expected, that the results of the calculated yield stress correlate to the measurements from the viscomat.

Table 4: Summary of sensor data during volume flow measurements

Mixture	Mix A	Mix B	Mix C	Mix D	Mix E
$\Delta P_{A,20\%}$ [bar]	0.39	0.36	0.35	0.41	0.15
$\Delta P_{A,50\%}$ [bar]	0.41	0.39	0.37	0.47	0.18
$\Delta P_{A,80\%}$ [bar]	0.43	0.43	0.43	0.53	0.21
$\Delta P_{B,20\%}$ [bar]	0.27	0.27	0.22	0.28	0.14
$\Delta P_{B,50\%}$ [bar]	0.30	0.30	0.25	0.22	0.16
$\Delta P_{B,80\%}$ [bar]	0.29	0.35	0.29	0.27	0.17
$Q_{20\%}$ [dm^{3}s^{-1}]	0.074	0.087	0.083	0.021	0.087
$Q_{50\%}$ [dm^{3}s^{-1}]	0.087	0.089	0.100	0.028	0.116
$Q_{80\%}$ [dm^{3}s^{-1}]	0.095	0.13	0.140	0.035	0.146
Temperature T1 [°C]	33.4	36.8	33.6	44.7	30.6
Temperature T2 [°C]	28.0	36.6	33.4	30.7	29.1

Apparently in most of the sub-figures, the correlation between most of the calculations and the data from the 'Viscomat NT' is not sufficient. Nevertheless, the results shown in Fig 3 e) seem to have a good indication of yield stress. These values are calculated for the longer pipe A with a distance between the sensors of 2.67 m and the higher variation in pump speed from 20 % to 80 %. In that specific constellation the calculations seem to be underestimating yield stress. For all except for Mix D, a higher yield stress given by the viscomat also leads to a higher calculated yield stress. In Fig. 3 f), which shows the calculations for the pipe B with 1.16 m between the pressure sensors P3 and P4, it appears that the calculations underestimate even more, except for Mix D. From the experimental data it could be observed, that the temperature in the circuit increases during pumping. For example the data in Fig 2 shows a rise in temperature of approximately $10\,K$ from the beginning of the experiment to the end. This significant increase in temperature is due to the high amount of friction in the worm pump. The mean temperature of the sensors during the flow measurements is listed in table 4. It can be expected, that the rheological properties of a fluid are varying with temperature [14]. This is not considered by the Buckingham-Reiner-equation. Therefore, a discrepancy of calculated yield stress in the pipe sections and determined yield stress in the viscomat can be expected. Furthermore, the temperature of Mix D was significantly higher compared to the rest of the mixtures, which could explain the even higher discrepancy of the calculated yield stress.

Comparing of viscosity. According to Tattersal et al., if α is calculated, the plastic viscosity can be calculated using the Buckingham-Reiner equation Eq. 5 [6]. The results for the calculations on viscosity are visualised in Fig. 4. Except for Mix D (which is the mixture with high temperature), it can be observed that Fig. 4 e) gives results that have a linear correlation, yet with a negative slope. Further investigations are necessary to perform calculations of viscosity during the experiments.

$$\frac{\Delta P}{l} = \frac{8\mu Q}{\pi r_{pipe}^4} \Big/ \left(1 - \frac{4\alpha}{3} + \frac{\alpha^4}{3}\right) \tag{5}$$

Comparison with flow table testing. Besides the rheological measurements, the spread flow of the tested mortars was determined and compared with the calculated values. Flow table testing has been performed during the experimental program to compare the results of the calculations with a conventional construction site method. The results are similar as shown above, once it is noted, that a lower yield stress results in higher flow in the flow table tests. Also it can be seen, that again only the comparison of pipe A with a pump speed variation of 20 % to 80 % shows calculated values that appear to be plausible. In Fig. 5 the data is plotted. The thin-lined cross indicates the measurements before the table was dropped 15 times, the cross with the wider lines afterwards respectively.

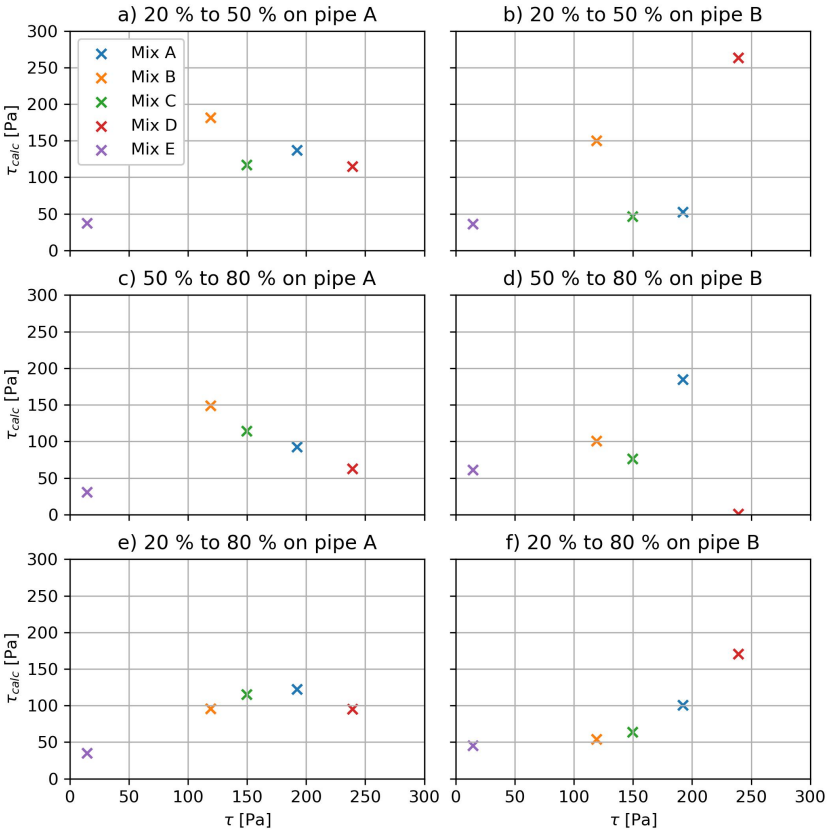

Fig. 3: Comparison between yield stress from ’Schleibinger Viscomat NT’ and calculated yield stress based on different levels of pump speed

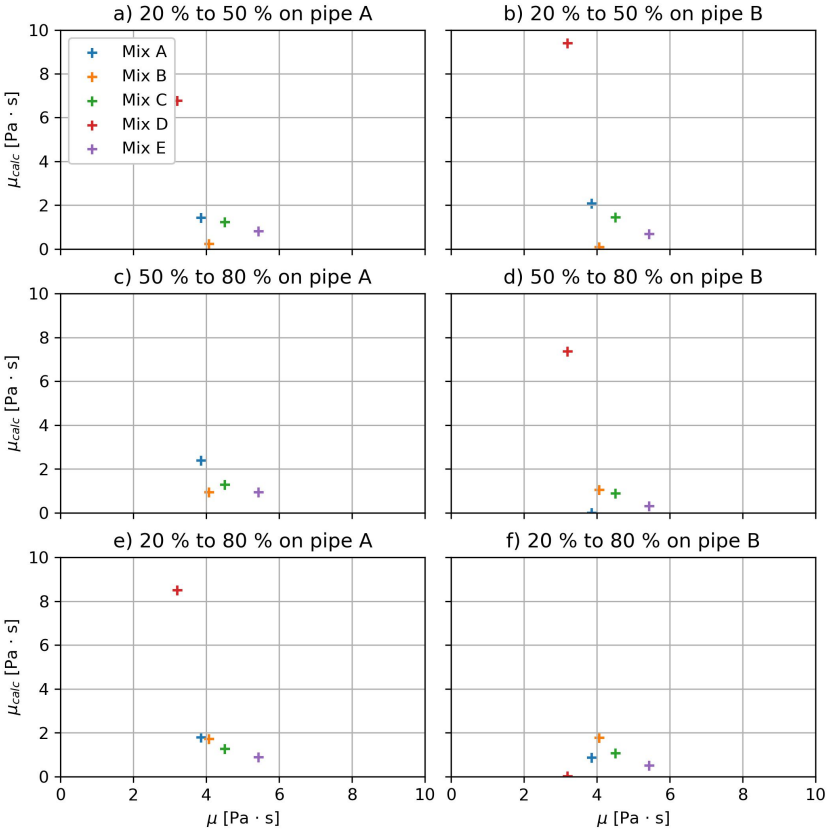

Fig. 4: Comparison of plastic viscosity from ’Schleibinger Viscomat NT’ and calculations based on different levels of pump speed

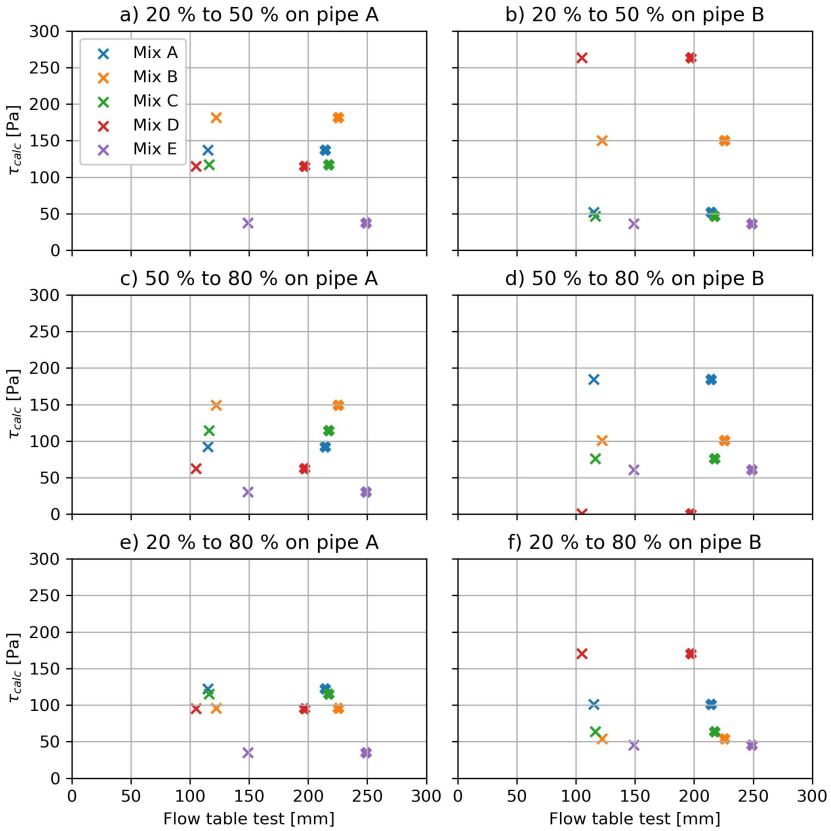

Fig. 5: Comparison between flow table testing and calculated yield stress based on different levels of pump speed

Conclusion

The experiments performed demonstrated that the yield stress of the mortars used can be determined by calculations using pressure data obtained by measurements performed in a rigid pipe. The corresponding calculations require the pressure loss in the system (determined by two pressure sensors placed at the inlet and the outlet of the pipe) and the volume flow at different flow rates (pumping speed). However, the experiments showed also that a continuous measurement of the volume flow and a significant difference in the considered volume flows are required. Furthermore, the length of the rigid pipe used for determining the pressure loss influences the accuracy of the calculations. The shorter the pipe, the lower the pressure loss and the higher the influence of measuring errors caused by the accuracy of the sensors. Further experiments will be performed to determine the temperature effect on the rheological properties calculated from the experimental data.
The variation of the pump speed during printing to a certain extent and the corresponding measurements to determine the pressure loss are a promising approach for a continuous quality control of the rheological parameters of the fresh mortar. Therefore, more investigations on calculating the viscosity from the experimental data are needed.

Summary

In this study, experiments on pressure loss in a rigid pipe were performed with a non-reactive limestone mixture. The scope was to investigate if continuous monitoring of pressure can be used for quality control in 3DCP. To achieve that, mixtures with different rheological properties were analysed using a rheometer and have been pumped in a curcuit with different volume flow. The calculations, based on the Buckingham-Reiner-equation show a good indication of yield stress and flow table testing if the difference in volume flow is significant.

Acknowledgements

The present work is part of a project funded by the Federal Ministry for Economic Affairs and Climate Action within the funding program TTP Leichtbau, grant number 03LB5005.

References

[1] S. Lim et al. “Developments in construction-scale additive manufacturing processes”. In: *Automation in Construction* 21 (2012), pp. 262–268. ISSN: 0926-5805. DOI: 10.1016/j.autcon.2011.06.010.

[2] Nathalie Labonnote et al. “Additive construction: State-of-the-art, challenges and opportunities”. In: *Automation in Construction* 72 (2016), pp. 347–366. ISSN: 09265805. DOI: 10.1016/j.autcon.2016.08.026.

[3] Theo A. M. Salet et al. “Design of a 3D printed concrete bridge by testing”. In: *Virtual and Physical Prototyping* 13.3 (2018), pp. 222–236. ISSN: 1745-2759 1745-2767. DOI: 10.1080/17452759.2018.1476064.

[4] Weiguo Xu et al. “Toward automated construction: The design-to-printing workflow for a robotic in-situ 3D printed house”. In: *Case Studies in Construction Materials* 17 (2022), e01442. ISSN: 2214-5095. DOI: https://doi.org/10.1016/j.cscm.2022.e01442. URL: https://www.sciencedirect.com/science/article/pii/S2214509522005745.

[5] Christoph Strangfeld et al. “Introduction of a monitoring system for Bingham fluids in additive manufacturing with concrete”. In: *International Symposium Non-Destructive Testing in Civil Engineering (NDTCE 2022)*, pp. 1–12. URL: https://opus4.kobv.de/opus4-bam/frontdoor/index/index/docId/55636%20https://nbn-resolving.org/urn:nbn:de:kobv:b43-556367.

[6] G. H. Tattersall and P. F. G Banfill. *The Rheology of Fresh Concrete*. PITMAN PUBLISHING INC, 1983. ISBN: 0-273-08558-1.

[7] M. A. Haustein, M. N. Kluwe, and R. Schwarze. “Experimental Investigation of the Pumping of a Model-Concrete through Pipes”. In: *Materials* 13.5 (2020). DOI: 10.3390/ma13051161.

[8] M. Sakuta. “PUMPABILITY AND RHEOLOGICAL PROPERTIE OF FRESH CONCRETE”. In: *Proceedings of Conference on Quality Control of Concrete Structures* (1979).

[9] European Committee for Standardization. *DIN EN 1015-7 Methods of test for mortar for masonry - Part 7: Determination of air content of fresh mortar*. Standard. 1998.

[10] M. Haist et al. “Interlaboratory study on rheological properties of cement pastes and reference substances: comparability of measurements performed with different rheometers and measurement geometries”. In: *Materials and Structures* 53.4 (2020). DOI: 10.1617/s11527-020-01477-w.

[11] European committee for standardization. *DIN EN 1015-3 Methods of test for mortar for masonry - Part 3: Determination of consistence of fresh mortar (by flow table)*. Standard. 2019.

[12] BIPM et al. *Evaluation of measurement data — Guide to the expression of uncertainty in measurement*. Joint Committee for Guides in Metrology, JCGM 100:2008. URL: https://www.bipm.org/documents/20126/2071204/JCGM%5C_100%5C_2008%5C_E.pdf/cb0ef43f-baa5-11cf-3f85-4dcd86f77bd6.

[13] European committee for standardization. *Industrial platinum resistance thermometers and platinum temperature sensors(IEC 60751:2008);German version EN 60751:2008*. Standard. 2009.

[14] Heinz Schade et al. “I-VIII”. In: *Strömungslehre*. Berlin • New York: De Gruyter, 2007, pp. I–VIII. ISBN: 9783110189728. DOI: doi:10.1515/9783110189728.fm.